Progress in Physics of Applied Materials 6 (2026), Serial Number 12, 179-192

Semnan University

Progress in Physics of Applied Materials

journal homepage: https://ppam.semnan.ac.ir/

Multifunctional Dye Interlayer Enhances the Power Conversion Efficiency of $Cs_2AgBiBr_6$ Lead-Free Inorganic Perovskite Solar Cell in a SCAPS-1D Simulation

E. Danladi[a*], D.S. Adepehin[a], A.O. Salawu[b], M.I. Amanyi[a], I.A. Ibrahim[c], O.E. Onah[a], E.A. Ogeh[a], F.A. Abumbe[a]

[a]*Department of Physics, Federal University of Health Sciences, Otukpo, Benue State, Nigeria*
[b]*Department of Computer Science, Nile University of Nigeria*
[c]*Department of Science Education, Federal University Dutsin-Ma, Katsina State, Nigeria*

ARTICLE INFO

Article history:
Received: 23 October 2025
Revised: 6 December 2025
Accepted: 20 December 2025
Published online: 10 January 2026

Keywords:
Perovskite solar cell;
SCAPS-1D;
N719 dye.

ABSTRACT

This study presents a simple, yet efficient method for improving the performance of $Cs_2AgBiBr_6$ perovskite solar cells (PSCs) by adding a N719 dye as an interlayer between the absorber and the hole transport layer (HTL). This was achieved through device simulation using solar capacitance simulation software in one dimension (SCAPS-1D), which based on Poisson and continuity equations. The presence of the N719 dye promotes faster hole extraction, improves energy level alignment within the device structure, decreases charge carrier recombination, and increases the range of light absorption. The open circuit voltage (V_{oc}), current density (J_{sc}), fill factor (FF), and power conversion efficiency (PCE) of the pure $Cs_2AgBiBr_6$-based device were 0.81V, 7.61 mA/cm^2, 46.68%, and 2.89%, respectively, whereas the V_{oc}, J_{sc}, FF, and PCE of the N719 modified $Cs_2AgBiBr_6$ device were 1.15 V, 8.05 mA/cm^2, 59.89%, and 5.53% respectively. Consequently, optimizing the electron transport layer (ETL) N_D, ETL *N*t, absorber layer band gap, thickness, and absorber *N*t, to obtain the optimal values of 10^{20} cm^{-3}, 10^{15} cm^{-2}, 1.9 eV, 0.4 µm, and 10^{11} cm^{-2}, respectively, led to achieve a remarkable PCE of 14.09%, which is a notable improvement over the $Cs_2AgBiBr_6$-based perovskite solar cells that have been previously documented in the literature.

1. Introduction

Organic-inorganic halide perovskite solar cells (PSCs) have garnered a lot of attention as possible next-generation photovoltaic technologies, since their first introduction by Kojima, et al. [1]. They are seen as great competitors to traditional devices like monocrystalline and polycrystalline silicon solar cells due to their cost effectiveness, simple manufacturing procedures, and potential for high power conversion efficiencies [2, 3].

Power conversion efficiency of PSCs has increased significantly over the last 14 years, reaching over 26% [4]. Despite these impressive advancements, a number of obstacles still hinder their commercialization viability, which include; current-voltage hysteresis, limited long-term stability, lead toxicity, and inadequate moisture resistance [5-8]. In order to mitigate these challenges, researchers have focused on all-inorganic, lead-free perovskites, which provide better stability and increased environmental compatibility. Cations like Sn^{2+}, Ge^{2+}, Bi^{3+}, and Sb^{3+} are environmentally safe alternatives for the hazardous divalent Pb^{2+} ion [9, 10], due to their similar ionic radii and electronic configurations. However, the stability of the material is compromised due to change in oxidation state of Sn^{2+} and Ge^{2+} to Sn^{2+} and Ge^{2+}, respectively [11]. Furthermore, low-dimensional $A^{+}{}_3B^{3+}{}_2X_9$ structures with

* Corresponding author.
E-mail address: danladielibako@gmail.com

Cite this article as:

Danladi, E., Adepehin, D.S., Salawu, A.O., Amanyi, M.I., Ibrahim, I.A., Onah, O.E., Ogeh, E.A. and Abumbe, F.A.,2026. Multifunctional Dye Interlayer Enhances the Power Conversion Efficiency of $Cs_2AgBiBr_6$ Lead-Free Inorganic Perovskite Solar Cell in a SCAPS-1D Simulation. *Progress in Physics of Applied Materials*, *6*(3), pp.179-192. DOI: **10.22075/ppam.2025.39482.1181**

suboptimal optoelectronic properties such as limited charge carrier mobility and high exciton binding energies are commonly formed by halide perovskites based on trivalent Bi^{3+} and Sb^{3+}, which ultimately result in low PCEs [12]. Halide double perovskites (HDPs) with the general formula $A^{+}{}_2B^{3+}X_6$ replaced the hazardous Pb^{2+} with the more ecologically friendly Bi^{3+} while maintaining the three-dimensional crystal structure. This structure substitutes one monovalent (B^{+}) and one trivalent (B^{3+}) cation for two divalent Pb^{2+} ions [12, 13]. $Cs_2AgBiBr_6$ has become a well-known HDP in recent years and has been synthesized successfully and used for energy conversion applications, including photovoltaics, photocatalysis, and photodetection [14, 15] . Using both vapor deposition and solution-based processing methods, several researchers have successfully fabricated $Cs_2AgBiBr_6$ thin films for perovskite solar cells [16-18]. Recent studies have also focused on other lead-free double perovskites, including $Cs_2AgInCl_6$, $Cs_2AgSbBr_6$, and $Cs_2NaBiCl_6$. The broad bandgap (~3.3 eV) of $Cs_2AgInCl_6$ prevents effective absorption of visible light, though with desirable optical tunability. Similarly, $Cs_2NaBiCl_6$ is unstable and has poor charge transport despite being environmentally benign. Although $Cs_2AgSbBr_6$ exhibits some promising features due to its narrower bandgap (~1.95–2.0 eV), its synthesis remains difficult, and only few reports on its device performance have been documented [19-21]. On the other hand, $Cs_2AgBiBr_6$ provides a moderate bandgap of about 2.15 eV, good thermal stability and ease of fabrication, making it a viable option for further improvement through interface modification and doping. For this study, $Cs_2AgBiBr_6$ was chosen as the absorber material [22]. Despite its favorable properties, the intrinsic characteristics of $Cs_2AgBiBr_6$, such as its wide indirect band gap, high charge carrier effective masses, restricted charge transport ability, and poor light absorption characteristics, continue to lower the efficiency of the device [23-25]. Extrinsic factors like the limited solubility of halide precursors in common organic solvents and the need for high annealing temperatures (usually above 250 °C) to achieve phase purity further complicate the production of high-quality, single-phase $Cs_2AgBiBr_6$ films. These challenges impede the formation of homogeneous perovskite layers, which are necessary to achieve high device efficiency. As a result, the highest PCE ever recorded for $Cs_2AgBiBr_6$-based PSCs is still only 6.37% [26], suggesting that lead-free $Cs_2AgBiBr_6$ PSCs requires more effort to improve their performance.

In this work, without changing the current device architecture, we suggest a simple method to improve the power conversion efficiency of $Cs_2AgBiBr_6$-based perovskite solar cells through the use of SCAPS-1D tool, which is based on the Poisson and equation of continuity that operates by iteratively solving fundamental semiconductor equations while accounting for the linear distribution of electron and hole concentrations. The fundamental idea is to modify the surface of $Cs_2AgBiBr_6$ films with an interfacial layer of N719 dye (di-tetrabutylammonium cis-bis (isothiocyanato) bis (2,2′-bipyridyl-4,4′-dicarboxylato) ruthenium (II)). The $Cs_2AgBiBr_6$ film's surface defects are passivated, the light absorption range is increased, and more effective hole extraction is made possible by this dye layer. With the addition of the N719 dye interlayer, the $Cs_2AgBiBr_6$-based perovskite solar cell achieved a PCE of 14.09%, along with an open-circuit voltage (V_{oc}) of 1.18 V, a fill factor (FF) of 76.56%, and a short-circuit current density (J_{sc}) of 15.56 $mAcm^{-2}$. This approach provides a simple and efficient way to improve the photoelectric performance of PSCs based on lead-free $Cs_2AgBiBr_6$. In addition, this work supports initiatives to reduce the overall carbon footprint by offering insightful information about cleaner and sustainable production methods in energy-related industries that use dye materials.

2. Theoretical Methods and Simulations

The simulation in this paper was carried out using the Solar capacitance simulation software in one dimension (SCAPS-1D), which was developed by Burgelman and his colleagues at the University of Ghent. Some of the benefits that have drawn a lot of attention to the SCAPS-1D tool include the user-friendliness, ability to simulate in both light and dark conditions, ability to simulate up to seven layers in the simulation environment without requiring standard capacitance-voltage and capacitance-frequency measurements, and ability to provide spectral response in terms of external quantum efficiency (EQE) [27]. The SCAPS package has been applied for different types of solar cells with different materials and structures, as well as having single junction or tandem configurations [28-31]. The tool solves the fundamental semiconductor equations iteratively while addressing the electron and hole concentrations linearly [10]. The input parameter needs to be carefully selected in order for the simulation to accurately represent its real counterpart. Equations 1-3 display the fundamental semiconductor equations [9].

$$\frac{d^2}{dx^2}\psi(x) = \frac{q}{\varepsilon_0\varepsilon_r}[p(x) - n(x) + N_D - N_A + \rho_P - \rho_n] \quad (1)$$

$$\frac{\partial n}{\partial t} = \frac{1}{q}\frac{\partial J_n}{\partial x} + (G_n - R_n) \quad (2)$$

$$\frac{\partial p}{\partial t} = \frac{1}{q}\frac{\partial J_p}{\partial x} + (G_p - R_p) \quad (3)$$

where ψ is the electrostatic field, n(x) is the electron carrier density, p(x) is the hole carrier density, Relative permittivity is denoted by ε_r, free-space permittivity by ε_0, donor impurity concentration by N_D, acceptor concentration by N_A, hole distribution by ρ_P, electron distribution by ρ_n, electric charge by q, rate of generation by G, rate of recombination by R, electron density by J_n, and hole density by J_p.

The device's efficiency and fill factor can be determined using equations 4 and 5.

$$FF = \frac{J_{mp}V_{mp}}{J_{sc}V_{oc}} \quad (4)$$

$$n = \frac{J_{sc}V_{oc}FF}{P_{in}} \quad (5)$$

where, J_{mp} = Maximum obtainable current, V_{mp} = Maximum obtainable voltage, J_{sc} = Short circuit current, V_{oc} = Open circuit voltage.

Standard conditions for the study included a temperature of 300 K, a frequency of $1x10^{16}$ Hz, and light illumination of 100 mW/cm^2. The HTL/$Cs_2AgBiBr_6$ interface was modified to include an interlayer in order to investigate the effects of interfacial recombination on photovoltaic performance. The data for the various layers are displayed in Table 1. The data for the defect interface is displayed in Table 2. The optical reflectance is considered to be zero at the surface and at all interfaces. The control variable method was used to optimize the parameters. The characteristic energy is set to 0.1 eV and a neutral Gaussian distribution defect is selected for the absorber layer.

Batch simulations were used to examine how layers' parameters affected the PSCs device. In particular, the effects of ETL N_D, ETL N_t, absorber layer band gap, absorber thickness, and N_t were investigated. Figure 1 displays the device structure, which was adopted from the work of Yang et al. [24] by employing N719 dye as an interlayer between the absorber and spiro-OMeTAD HTL to increase the light absorption range, minimize recombination and stop degradation, and more effective hole extraction is made possible by this dye layer. The FTO/TiO_2/$Cs_2AgBiBr_6$/spiro-OMeTAD/BC and FTO/TiO_2/$Cs_2AgBiBr_6$/dye/spiro-OMeTAD/BC configurations serve as the foundation for the devices. The fluorine tin oxide (FTO) contact provided the device's illumination, TiO_2 transports electrons, $Cs_2AgBiBr_6$ acts as an absorber, and spiro-OMeTAD transports holes. 4.4 and 4.94 eV are the FTO and BC work functions, respectively [32].

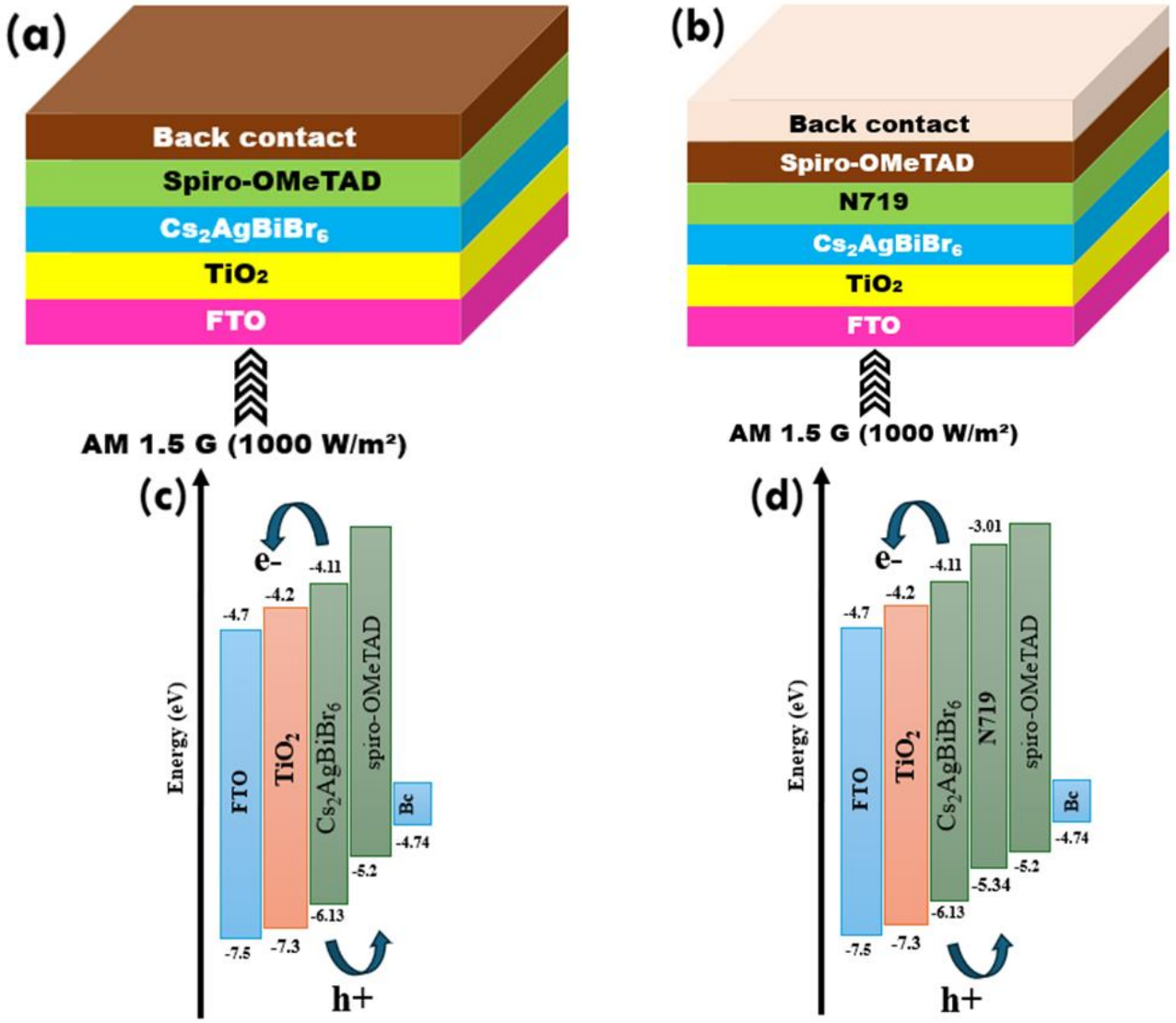

Fig. 1. (a) Solar cell configuration without N719, (b) Solar cell configuration with N719, (c) The energy-band without N719, and (d) The energy-band with N719.

Table 1. Data for individual layer used for the simulation of the PSC [3, 21, 33, 34].

Parameters	FTO	TiO_2	$Cs_2AgBiBr_6$	N719	Spiro
T (μm)	0.3	0.05	0.4	0.6	0.3
E_g (eV)	3.5	3.2	2.1	2.33	2.9
χ (eV)	4.0	4.2	4.26	3.9	2.2
ϵ_r	9.0	10.0	5.8	30	3.0
N_C (cm^{-3})	2.2×10^{18}	2.2×10^{18}	1.0×10^{19}	2.4×10^{20}	2.2×10^{18}
N_V (cm^{-3})	1.8×10^{18}	1.8×10^{19}	1.0×10^{19}	2.5×10^{20}	1.8×10^{19}
μ_n ($cm^2\ V^{-1}\ s^{-1}$)	20	20	11.81	5	2.0×10^{-4}
μ_p ($cm^2\ V^{-1}\ s^{-1}$)	10	10	0.49	5	2.0×10^{-6}
e v_{th} (cm/s)	1×10^{7}	1×10^{7}	1×10^{7}	1×10^{7}	1×10^{7}
h v_{th} (cm/s)	1×10^{7}	1×10^{7}	1×10^{7}	1×10^{7}	1×10^{7}
N_D (cm^{-3})	2×10^{19}	1×10^{17}	1×10^{16}	0	0
N_A (cm^{-3})	0	0	1×10^{16}	1×10^{17}	1.0×10^{19}
N_t (cm^{-3})	1×10^{15}	1×10^{15}	1×10^{14}	1×10^{15}	1×10^{15}

Table 2. Data used for the interface layer.

Parameters	Absorber	ETL/$Cs_2AgBiBr_6$	dye/$Cs_2AgBiBr_6$	HTL/dye	HTL/$Cs_2AgBiBr_6$
Defect type	Neutral	Neutral	Neutral	Neutral	Neutral
σ (e) (cm^2)	1×10^{-15}	2×10^{-16}	2×10^{-16}	1×10^{-19}	1×10^{-19}
σ (h) (cm^2)	1×10^{-15}	2×10^{-16}	2×10^{-16}	1×10^{-19}	1×10^{-19}
Energetic distribution	Gaussian	Single	Single	Single	Single
Energy level with respect to Ev (eV)	0.600	0.600	0.600	0.600	0.600
Characteristic energy (eV)	0.1	0.1	0.1	0.1	0.1
N_t (cm^{-3})	1×10^{14}	1×10^{7}	1×10^{7}	1×10^{10}	1×10^{10}

3. Results and Discussion

3.1. Initial measurement and validation with and without N719

To ensure the precision and reliability of our simulation, we first replicated the dye-free device structure (FTO/TiO_2/$Cs_2AgBiBr_6$/Spiro-OMeTAD/BC) published by Yang et al. [24] using the parameters listed in Table 1. The simulated results were then compared with experimental and literature-based results, as indicated in Table 3. The strong agreement between our results and the experimental results shows the validity of the simulation approach. The *J-V* and *P-V* curves are shown in Figures 2a and b.

By placing a N719 dye between the Spiro-OMeTAD and the perovskite absorber, the performance of the PSC was enhanced in contrast to the dye-free configuration. The cell without the dye interlayer had a PCE of 2.89% with FF of 46.68%, J_{sc} of 7.61 mA/cm^2, and V_{oc} of 0.81 V. The cell with the N719 dye interlayer, on the other hand, showed a PCE of 5.53%, FF of 59.89%, J_{sc} of 8.05 mA/cm^2, and V_{oc} of 1.15 V. The efficiency has increased by about 1.91 times compared to the former. The N719 interlayer between the hole transport layer (HTL) and the perovskite absorber improves the photovoltaic performance parameters by improving interfacial charge dynamics and reducing energy losses. The N719 layer serves as an efficient charge mediator by preventing charge recombination at the interface and promoting hole extraction from the perovskite to the HTL. Furthermore, the N719 interlayer reduces leakage currents and non-radiative recombination by passivating surface defects at the perovskite/HTL interface [35]. This leads to improved FF and PCE as a result of improved charge transfer and decreased resistive losses. Also, the higher V_{oc} is due to decreased recombination, and the increased J_{sc} is due to more effective carrier collection.

Through energy band studies, as illustrated in Figures 2c and d, we further investigated the effects of adding N719 to the device. According to the energy band diagram, the N719-based device had an offset at the $Cs_2AgBiBr_6$/N719 interface that the dye-free device did not have. According to a detailed analysis of the energy band profile, the dye-containing device should have a lower resistance at the ETL/$Cs_2AgBiBr_6$ than the device without N719. Consequently, the dye-interlayered device is being considered for additional simulation.

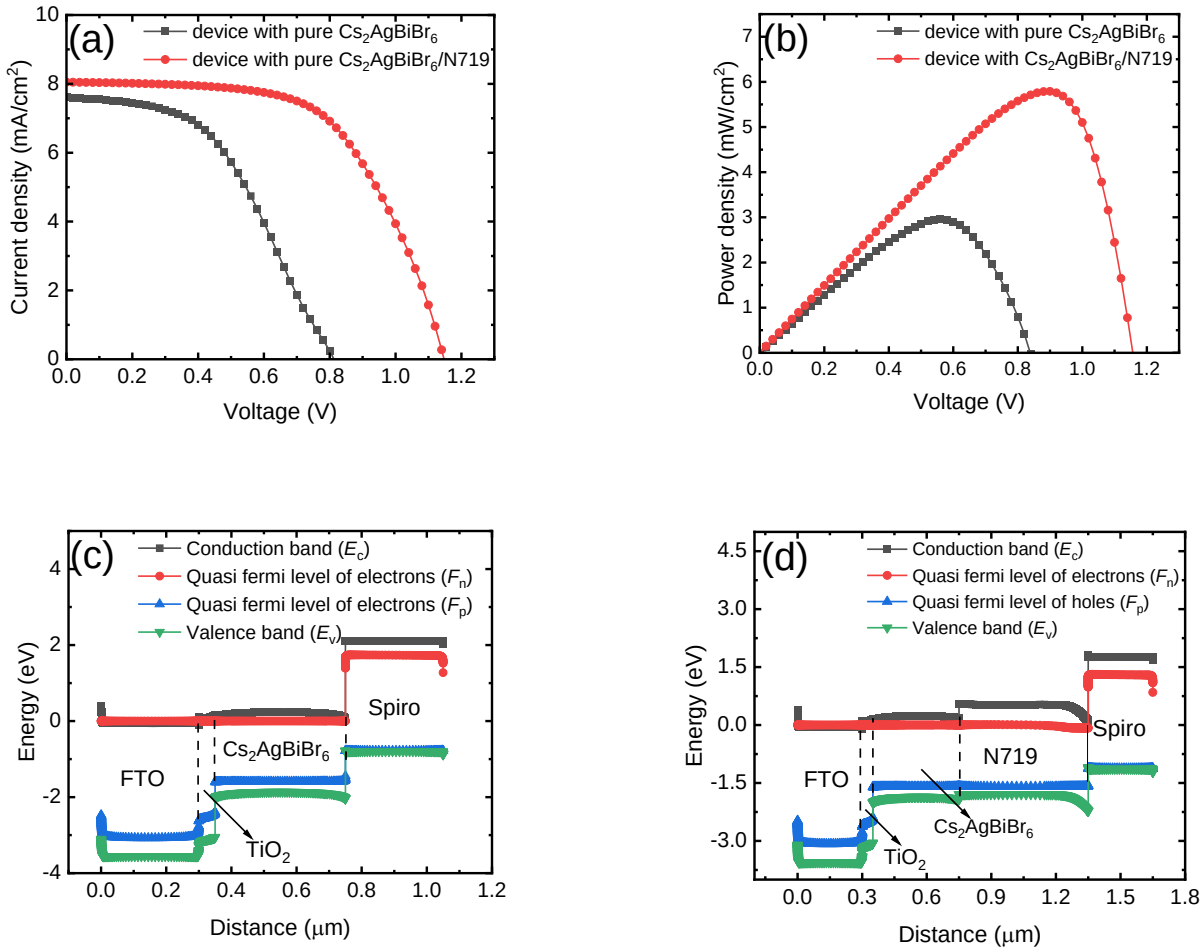

Fig. 2. (a) *J-V* curve with and without N719, (b) *P-V* curve with and without N719, (c) Energy band profile for device without N719, (d) Energy band profile for device with N719.

Table 3. *J-V* parameters of experimental and simulated outcomes.

Device	PCE (%)	*FF* (%)	J_{sc} (mA/cm²)	V_{oc} (V)	Remark
Experimental without N719	2.47	55.10	4.49	1.00	[24]
Experimental with N719	2.84	52.40	5.13	1.02	[24]
Simulation without N719	2.89	46.68	7.61	0.81	This work
Simulation with N719	5.53	59.89	8.05	1.15	This work

3.2. Effect of ETL N_D

The performance of the perovskite device is impacted by the N_D of the ETL. In this subsection, we examined the impact of ETL N_D on the photovoltaic metrics of the PSC by altering the N_D from 10^{15} to 10^{20} cm^{-3}. Figure 3a shows the *J-V* curve with different ETL N_D, and Figures 3b and c show the correlation between the PV parameters and the ETL N_D. According to Table 4 and the curves, the PCE and FF rise from 5.53 to 5.55% and from 59.79 to 60.04% with increase in the ETL N_D, respectively. The perovskite solar cell's PCE and FF increase as the N_D in the electron transport layer rises due to improved charge transport and decreased resistive losses [21]. A higher N_D improves the ETL's electrical conductivity and lowers the series resistance by increasing the number of free electrons in the ETL. As a result, electrons can be extracted from the perovskite absorber to the electrode more quickly and effectively. Furthermore, improved energy level alignment at the ETL/perovskite interface results from the upward shift of the ETL Fermi level caused by increase in doping [35]. This lowers the potential barrier for electron transfer and inhibits interfacial recombination. Excessive doping caused space charge regions to be formed close to the ETL/perovskite interface, trapping charge carriers and preventing them from adding to the photocurrent.

The open-circuit voltage and short-circuit current density remain constant as the ETL N_D rises because the ETL largely affects charge transport rather than light absorption or carrier generation [10]. The perovskite absorber layer, which remains unchanged as N_D rises, primarily controls the optical characteristics and photogeneration of charge carriers. Similarly, once effective charge extraction is attained, moderate changes in ETL doping have little effect on V_{oc}, which is primarily determined by the difference between the quasi-Fermi levels of electrons and holes in the device. As a result, higher N_D has little effect on J_{sc} and V_{oc},

which remain nearly constant, but it enhances conductivity and lowers series resistance (affecting FF and PCE). The optimized device's PCE, FF, J_{sc}, and V_{oc} are respectively 5.55%, 60.04%, 8.05 mA/cm^2, and 1.15 V which is at ETL N_D of 10^{20} cm^{-3}.

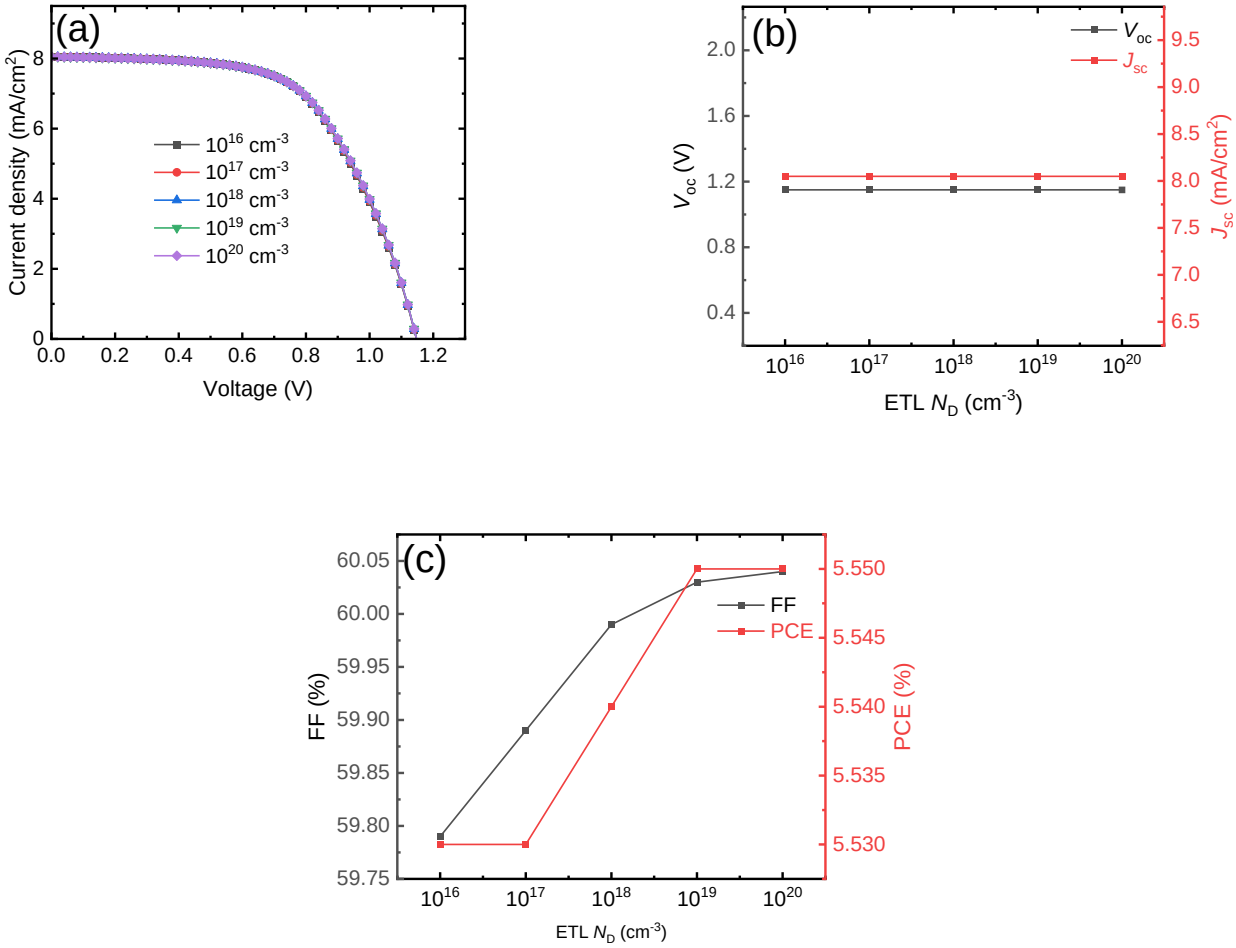

Fig. 3. (a) *J-V* curve, and correlation between (b) J_{sc} and V_{oc}, and (c) PCE and FF with ETL N_D.

Table 4. Effect of various ETL N_D.

ETL N_D (cm^{-3})	V_{oc} (V)	J_{sc} (mA/cm^2)	FF (%)	PCE (%)
10^{16}	1.15	8.05	59.79	5.53
10^{17}	1.15	8.05	59.89	5.53
10^{18}	1.15	8.05	59.99	5.54
10^{19}	1.15	8.05	60.03	5.55
10^{20}	1.15	8.05	60.04	5.55

3.3. Effect of ETL N_t

The ETL is a crucial layer of PSC and has a great impact on the performance of the device [3, 36]. The ETL defect density was varied from 10^{13} to 10^{17} cm^{-2}, and the parameters FF, PCE, V_{oc}, and J_{sc} were evaluated. Figure 4a shows the *J-V* curve with varied N_t. Figure 4b shows the relationship between FF and PCE, while Figure 4c shows the relationship between V_{oc} and J_{sc} with varied ETL N_t. The outcome of the study shows that the ETL is effective at all N_t during the simulation and has the ability to function effectively in the proposed architectural configuration (see Table 5). This indicates that the charge carrier diffusion length and carrier lifetime within the perovskite layer are often unaffected by the ETL N_t. As a result, it is unlikely that a change in ETL N_t will have an influence on the charge carrier diffusion length or carrier lifetime within the perovskite layer. It's crucial to note that, variation in the ETL N_t can also have an indirect impact on device performance by changing other factors such as charge extraction efficiency, contact resistance, or the interfacial impacts between the ETL and other layers.

3.4. Effect of absorber N_t

The absorber N_t is another crucial factor that must be considered in order to develop the best possible device. It is known that the absorber contains surface or bulk defects, which may be interstitial, Schottky, Frenkel, or vacancy

defects [10]. Furthermore, the absorber may also have additional defects like dislocations and grain boundaries [37]. According to some research, self-doping, which makes up the p-type semiconductor, causes defects in the perovskite absorber due to impurity [21, 38, 39]. The band gap may become shallower or deeper as a result of these defects. These defects have the potential to trap charge carriers and promote non-radiative recombination. Perovskite morphology and film quality have an impact on PSC metrics [40], this has also been shown that recombination inside the perovskite layer is prominent when the ETL has low quality and film coverage, which affects the V_{oc}. To find the best-performing device, the effect of changing absorber N_t from 10^{11} to 10^{15} cm^{-2} was examined in this study. The *J-V* plot with varied absorber N_t is shown in Figure 5a while the relationship between J_{sc} and V_{oc} with N_t and PCE and FF with N_t are shown in Figures 5b and c, respectively. As absorber N_t increases, all of the photovoltaic parameters decrease (see Table 6). This decrease is attributed to interface recombination or trap-assisted SRH. The shorter diffusion lengths which is caused by an increase in absorber N_t is responsible for the low efficiency which increases carrier loss due recombination [41]. This implies that when absorber N_t increases, so does the rate of carrier recombination, which accelerates solar cell degradation and lowers performance. The absorber's optimized N_t of 10^{11} cm^{-2} was chosen for further simulation.

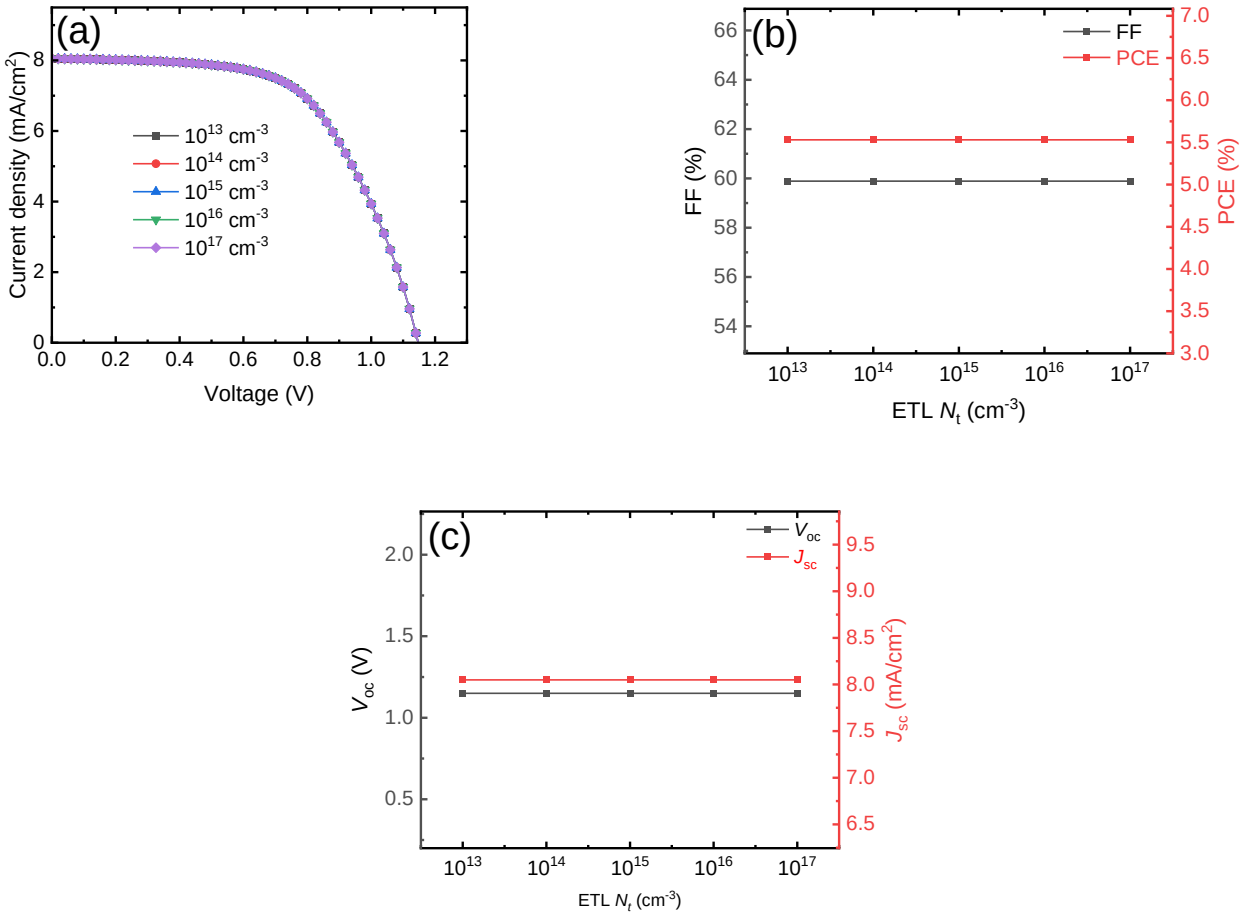

Fig. 4. (a) *J-V* curve, and correlation between (b) PCE and FF, and (c) J_{sc} and V_{oc} with ETL N_t.

Table 5. Effect of varying ETL N_t.

ETL N_t (cm^{-3})	V_{oc} (V)	J_{sc} (mA/cm^2)	FF (%)	PCE (%)
10^{13}	1.15	8.05	59.89	5.53
10^{14}	1.15	8.05	59.89	5.53
10^{15}	1.15	8.05	59.89	5.53
10^{16}	1.15	8.05	59.89	5.53
10^{17}	1.15	8.05	59.89	5.53

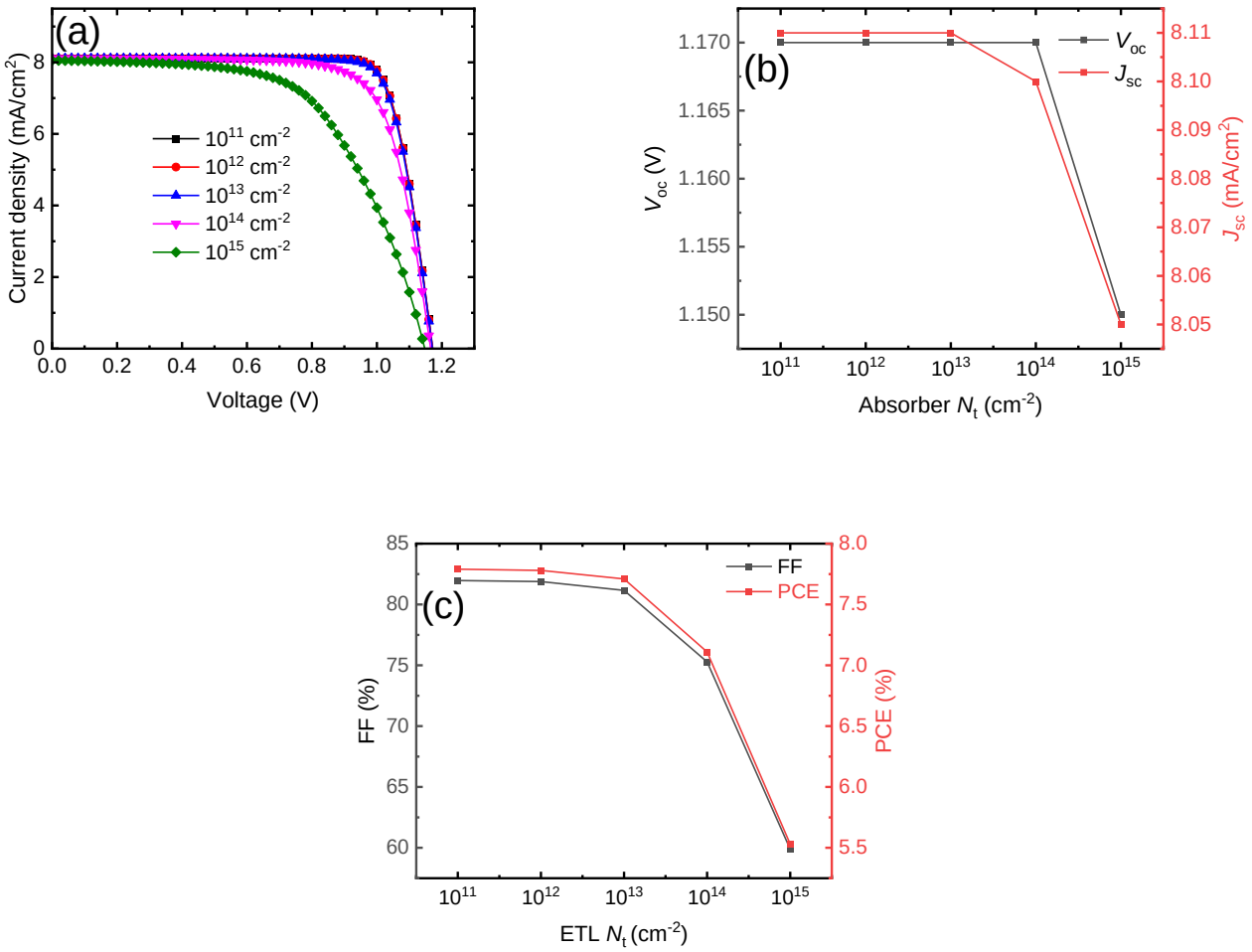

Fig. 5. (a) *J-V* curve, and correlation between (b) J_{sc} and V_{oc}, and (c) PCE and FF with absorber N_t.

Table 6. Effect of varying different Absorber N_t.

Absorber N_t (cm^{-3})	V_{oc} (V)	J_{sc} (mA/cm^2)	FF (%)	PCE (%)
10^{11}	1.17	8.11	81.97	7.79
10^{12}	1.17	8.11	81.88	7.78
10^{13}	1.17	8.11	81.16	7.71
10^{14}	1.17	8.10	75.28	7.11
10^{15}	1.15	8.05	59.89	5.53

3.5. Effect of absorber thickness

One of the key elements that affects PSC performance is the thickness of the absorber layer; and therefore, it must be carefully chosen for the device to work optimally. If the thickness is too thin, the PSC device might not absorb all of the energetic photons that strike it, and if it is too thick, it will cause recombination channels to be formed within it [42]. In this subsection, all other parameters were kept constant while the thickness was varied from 0.1 to 0.7 µm. Within this range only three values converged during the simulation, while all other values show failure in convergence. The device's *J-V* plots with varying thicknesses are shown in Figure 6a. Comparison between J_{sc} & V_{oc} is shown in Figure 6b, while comparison between PCE & FF is shown in Figure 6c. All the photovoltaic data with different absorber thicknesses are compared in Table 7. According to the results, when the thickness of the absorbing material increases from 0.1 to 0.7 µm, the J_{sc} increases from 6.20 to 8.05 mA/cm^2, which is attributed to the high absorption coefficient of the perovskite absorber [21]. This means that thicker absorbers provide a large interactive area for light absorption, while thinner absorbers provide less active area for light absorption. The higher electron-hole recombination in the thicker absorber (0.7 µm) may be the cause of the decrease in V_{oc} [43, 44] . As absorber thickness increases, the FF steadily decreases, which is explained by an increase in series resistance [45]. In terms of the PCE, it first increased from 5.87% at 0.1 µm to 6.08% at 0.4 µm, and then it declined to 5.53% at 0.7 µm. This behavior can be explained as follows: at first, the absorber's thickness (0.1 to 0.4 µm) was less than the hole and electron diffusion lengths, which allowed the charge carriers to reach the electrodes and increased the PCE. PCE

decreases as a result of enhanced carrier recombination when the thickness surpasses 0.4 μm [43, 46] . This indicates that high resistance is created when moving charge carriers to the front/back contacts at layers larger than 0.4 μm [21]. The optimized thickness was chosen at 0.4 μm and used for further simulation.

3.6. Effect of absorber bandgap

The band gap of the absorber layer directly affects both light absorption and charge carrier transport, making it a critical factor in assessing the overall performance of perovskite solar cells. In this work, the band gap was varied between 1.9 and 2.3 eV during the simulation. The current-voltage curves of the solar cells are shown in Figure 7a. Comparison between J_{sc} & V_{oc} is shown in Figure 7b, while comparison between PCE & FF is shown in Figure 7c. The *J-V* curve shape is affected by numerous variables, such as the intrinsic qualities of the materials, the device architecture, lighting conditions, and operating temperature [47]. This curve can be used to determine key photovoltaic parameters, including PCE, FF, V_{oc}, and J_{sc}. It is clear that variations in the band gap have a great impact on these parameters, which highlights how important band-gap tuning is for maximizing device performance.

The J_{sc} and PCE of the perovskite solar cells decrease as the band gap rises from 1.9 to 2.3 eV. This is because only higher-energy (shorter wavelength) photons can be absorbed, while lower-energy photons pass through without aiding in the formation of photoexcited carriers. The decrease in the photogenerated charge carriers is responsible for the lower J_{sc} and worse overall device performance.

The FF of the perovskite solar cells fluctuate with changes in band gap, this is because the electronic characteristics of the absorber affect the interaction between charge transport, recombination, and resistive losses [48]. Higher photocurrent generation can intensify the effect of series resistance at intermediate band gaps, resulting in a minor decrease in FF. As the band gap widens, less carrier generation results in a lower current density, which temporarily improves FF due to fewer resistive losses. However, interfacial energy misalignments, higher defect densities, and noticeable non-radiative recombination are common problems for wide-band-gap perovskites [47, 49]. These elements increase recombination losses and prevent effective charge extraction, which eventually causes FF to decline (see Table 8). The combined effects of improved resistive behavior at intermediate band gaps and increased recombination losses at higher band gaps cause the fill factor to fluctuate rather than change uniformly as the band gap increases. The optimized band gap was 1.9 eV and was used for further simulation.

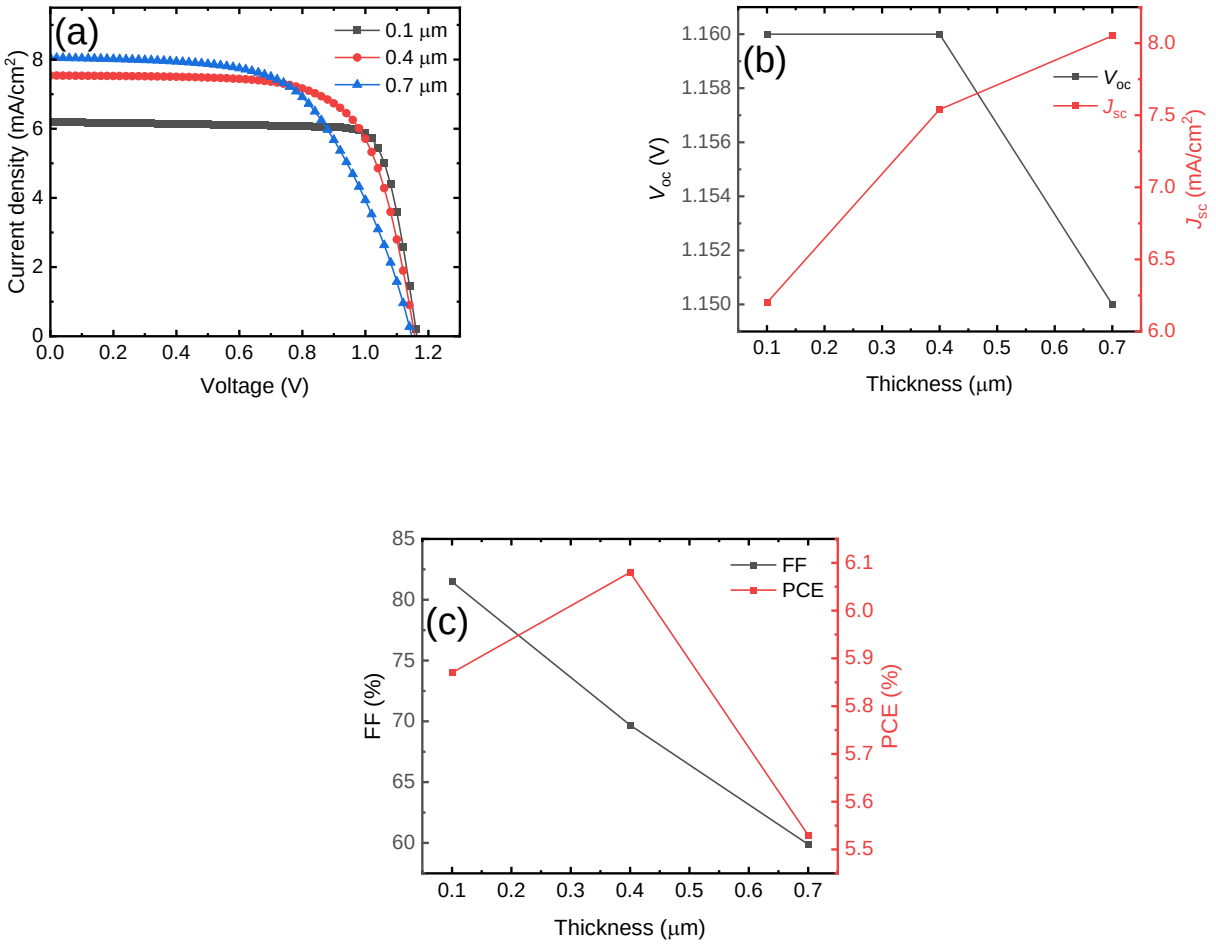

Fig. 6. (a) *J-V* curve, and (b) correlation between (b) J_{sc} and V_{oc}, and (c) PCE and FF with absorber thickness.

Table 7. Effect of varying absorber thickness.

Absorber thickness	V_{oc} (V)	J_{sc} (mA/cm²)	FF (%)	PCE (%)
0.1	1.16	6.20	81.47	5.87
0.4	1.16	7.54	69.69	6.08
0.7	1.15	8.05	59.89	5.53

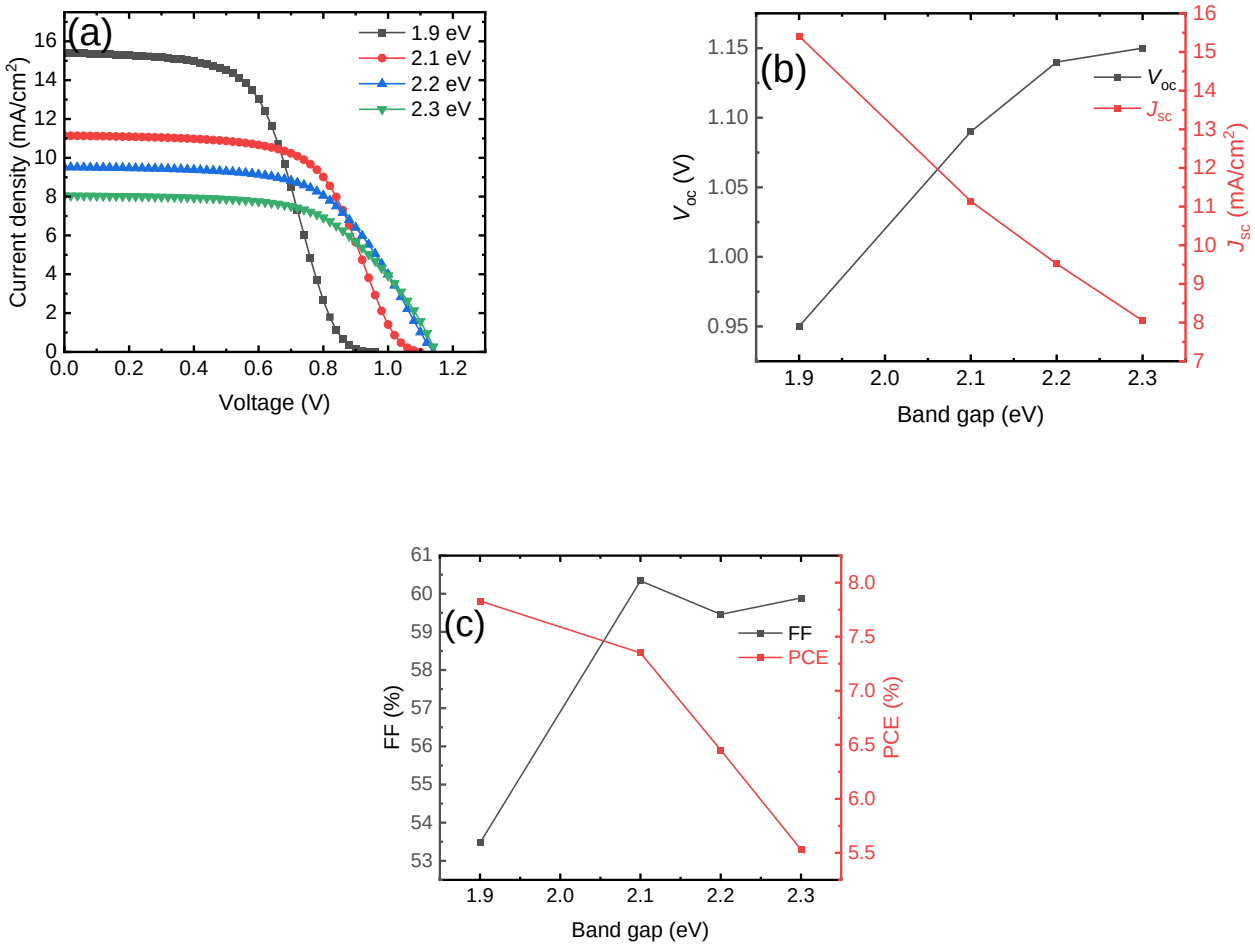

Fig. 7. (a) *J-V* curve, and (b) correlation between (b) J_{sc} and V_{oc}, and (c) PCE and FF absorber band gap.

Table 8. Effect of varying absorber band gap.

Absorber band gap	V_{oc} (V)	J_{sc} (mA/cm²)	FF (%)	PCE (%)
1.9	0.95	15.41	53.47	7.83
2.1	1.09	11.14	60.34	7.35
2.2	1.14	9.52	59.46	6.45
2.3	1.15	8.05	59.89	5.53

3.7. Optimized device

Optimal values were found after a careful analysis of the different layer parameters, and these were subsequently applied to further simulate the final device. The ETL N_D, optimal thickness and ETL N_t were found to be 10^{20} cm^{-3} and 10^{15} cm^{-2}, respectively. Similarly, the absorber layer band gap, thickness, and N_t were optimized with respective values of 1.9 eV, 0.4 µm, and 10^{11} cm^{-2}. The simulated device parameters with this optimized device were FF of 76.56%, V_{oc} of 1.18 V, maximum PCE of 14.09%, and J_{sc} of 15.56 mA/cm². The *J–V* characteristics of both optimized and unoptimized devices are displayed in Figure 8.

3.8. Comparison of our SCAPS-1D results with other results previously reported

The comparison of theoretical and experimental studies using our current simulation is shown in Table 9. All of the experimental results are noticeably worse than the simulation results. Previous simulation studies showed that it would take a lot of effort to achieve a comparable

trademark for lead-free PSCs. To date, $Cs_2AgBiBr_6$ perovskite solar cells have so far shown the highest efficiency of 6.37%, FF of 60.93%, J_{sc} of 11.4 mA/cm^2, and V_{oc} of 0.92 V. After employing an N719 dye interlayer in our simulation, the device demonstrated an optimized efficiency of 14.09%, FF of 76.56%, J_{sc} of 15.56 mA/cm^2, and V_{oc} of 1.18 V in the configuration FTO/TiO_2/$Cs_2AgBiBr_6$/N719/spiro-OMeTAD/BC. By simply integrating a layer of N719 between $Cs_2AgBiBr_6$ and spiro-OMeTAD, this study demonstrates better performance than previously published data and has opened a new avenue for achieving improved performance.

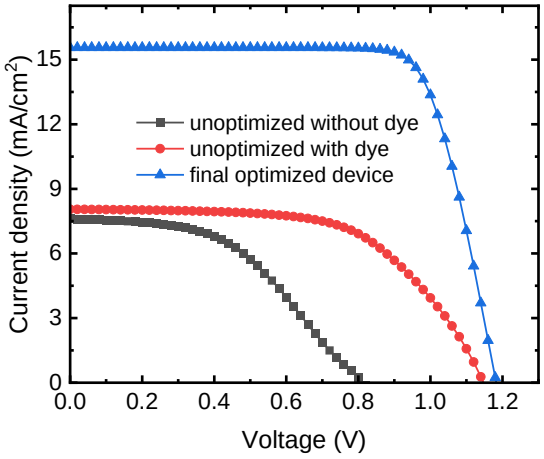

Fig. 8. *J-V* for the unoptimized and optimized devices.

Table 9. *J-V* data from present study and previously published literature.

Device	Study	V_{oc} (V)	J_{sc} (mA/cm^2)	FF (%)	PCE (%)	References
FTO/TiO_2/$Cs_2AgBiBr_6$/Spiro-OMeTAD/Ag	Exp	1.00	4.49	55.10	2.47	[24]
FTO/TiO_2/$Cs_2AgBiBr6$/N719/Spiro-OMeTAD/Ag	Exp	1.02	5.13	52.40	2.84	[24]
FTO/TiO_2/$Cs_{1.96}li_{0.01}Na_{0.03}AgBiBr_6$/C	Exp	1.02	3.29	54.30	1.82	[50]
FTO/TiO_2/$Cs_{1.96}li_{0.01}Na_{0.03}AgBiBr_6$/C	Exp	1.07	6.56	71.60	5.02	[50]
FTO/TiO_2/$Cs_2Ag_{0.95}GD_{0.05}BiBr_6$/spiro-OMeTAD/au	Exp	0.91	5.58	75.00	3.74	[20]
FTO/Ti/ZTO-$Cs_2Ag_{0.95}Mg_{0.05}BiBr_6$/Au	Exp	0.91	5.40	81.10	3.98	[19]
FTO/TO_2/$Cs_2AgBiBr_6$/C	Exp	0.43	9.4	38.00	1.63	[51]
ITO/SnO_2/$Cs_2AgBiBr_6$/spiro-OMeTAD/Au	Exp	0.92	11.4	60.93	6.37	[26]
FTO/TiO_2/Mo-$Cs_2AgBiBr_6$/Spiro-OMeTAD/Au	Exp.	0.94	5.59	67.00	3.95	[22]
FTO/TiO_2/$Cs_2Ag_{0.95}Pr_{0.05}BiBr_6$/P3HT/Spiro-OMeTAD	Exp.	0.90	5.01	81.1	3.88	[19]
FTO/TiO_2/IDL/$Cs_2AgBiBr_6$/C	Sim.	1.69	12.11	88.79	18.21	[52]
ITO/SnO_2/$Cs_2AgBiBr_6$/P3HT/Au	Sim.	2.02	6.39	90.0	11.32	[53]
FTO/SnO_2/$Cs_2AgBiBr_6$/Spiro-OMeTAD/Au	Sim.	1.30	17.44	62.59	14.29	[54]
ITO/CdS/$Cs_2AgBiBr_6$/$CuAlO_2$/Pt	Sim.	1.64	4.91	88.74	7.16	[55]
FTO/ZnSe/$CH_3NH_3SnI_3$/Graphene/Pt	Sim.	0.93	31.81	78.45	23.18	[56]
FTO/TiO_2/$Cs_2AgBiBr_6$/N719/Spiro-OMeTAD/BC	Sim.	1.18	15.56	76.56	14.09	This work

4. Conclusions

This study offers a comprehensive photovoltaic analysis of $Cs_2AgBiBr_6$ perovskite solar cells using the SCAPS-1D tool. The research was conducted to determine the effect of introducing N719 dye as an interlayer between $Cs_2AgBiBr_6$ and Spiro-OMeTAD on the photovoltaic performance. The pure PSC structure without N719 dye yielded a V_{oc} of 0.81V, J_{sc} of 7.61 mA/cm^2, FF of 46.68%, and PCE of 2.89%. A similar structure with N719 dye was simulated and a V_{oc} = 1.15 V, J_{sc} = 8.05 mA/cm^2, FF = 59.89%, and PCE = 5.53% were obtained. After optimizing the ETL N_D, ETL N_t, absorber layer band gap, thickness, and N_t, their values of 10^{20} cm^{-3}, 10^{15} cm^{-2}, 1.9 eV, 0.4 µm, and 10^{11} cm^{-2} were obtained respectively. The simulated device with these optimized parameters were FF of 76.56%, V_{oc} of 1.18 V, maximum PCE of 14.09%, and J_{sc} of 15.56 mA/cm^2. This

work has the potential to reduce carbon emissions by offering new scientific insights for cleaner production methods in industries that use perovskite materials for the larger energy sector.

Acknowledgement

The authors would like to thank Professor Marc Burgelman and his team from the Department of Electronics and Information Systems, University of Ghent, Belgium, for the development of the SCAPS software package and allowing its use.

Funding Statement

This research work was funded by "Tertiary Education Trust Fund (TETFUND) 2024 intervention" under grant number "2024/FX302-IBR".

Conflicts of interest

The authors declare that they have no known competing financial interests or personal relationships that could have appeared to influence the work reported in this paper.

Authors contribution statement

All authors contributed equally to this work.

Data availability statement

The data that support this paper will be made available upon reasonable request.

References

[1] Kojima, A., Teshima, K., Shirai, Y. and Miyasaka, T., 2009. Organometal halide perovskites as visible-light sensitizers for photovoltaic cells. *Journal of the american chemical society*, *131*(17), pp.6050-6051.

[2] Singh, A., Umakanth, V., Tyagi, N., Baghel, A.K. and Kumar, S., 2023. Comparative study of commercial crystalline solar cells. *Results in Optics*, *11*, p.100379.

[3] Danladi, E., Jubu, P.R., Tighezza, A.M., Hossain, I., Tasie, N.N., Abdulmalik, M.O., Egbugha, A.C., Awoji, M.O., Kashif, M., Onoja, E.D. and Amanyi, M.I., 2023. Highly efficient, hole transport layer (HTL)-free perovskite solar cell based on lithium-doped electron transport layer by device simulation. *Emergent Materials*, *6*(6), pp.1779-1795.

[4] Jiao, B., Tan, L., Ye, Y., Ren, N., Li, M., Li, H., Li, X. and Yi, C., 2025. One-stone-two-birds: over 26% efficiency in perovskite solar cells via synergistic crystallization & interface regulation. *Energy & Environmental Science*, *18*(11), pp.5437-5447.

[5] Danladi, E., Ichoja, A., Onoja, E.D., Adepehin, D.S., Onwoke, E.E., Ekwu, O.M. and Alfred, D.O., 2023. Broad-band-enhanced and minimal hysteresis perovskite solar cells with interfacial coating of biogenic plasmonic light trapping silver nanoparticles. *Materials Research Innovations*, *27*(7), pp.521-536.

[6] Danladi, E., Kashif, M., Ichoja, A. and Ayiya, B.B., 2023. Modeling of a Sn-based HTM-free perovskite solar cell using a one-dimensional solar cell capacitance simulator tool. *Transactions of Tianjin University*, *29*(1), pp.62-72.

[7] Sun, C., Xu, L., Lai, X., Li, Z. and He, M., 2021. Advanced Strategies of Passivating Perovskite Defects for High-Performance Solar Cells. *Energy & Environmental Materials*, *4*(3), pp.293-301.

[8] Ávila-López, A., Cruz, J.C., Díaz-Real, J.A., García-Uitz, K., Cante-Góngora, D. and Rodríguez-May, G., 2025. A Review of Perovskite-Based Solar Cells over the Last Decade: The Evolution of the Hole Transport Layer and the Use of WO_3 as an Electron Transport Layer. *Coatings*, *15*(2), p.132.

[9] Ogunmoye, K.A., Izang, J.C., Olorunyolemi, I., Ozurumba, A.C. and Danladi, E., 2025. Highly efficient MAGeI3 HTL-free perovskite solar cell with lithium-doped electron transport layer: A dive into SCAPS-1D simulation insight. *Journal of Energy Technology and Environment*, *7*(2), pp.34-50.

[10] Danladi, E., Obagboye, L.F., Aisida, S., Ezema, F.I., Okorie, O., Bwamba, J.A., Emmanuel, P.A., Hussaini, A.A., Jubu, P.R. and Ozurumba, A.C., 2025. 20.730% highly efficient lead-free CsSnI3-based perovskite solar cells with various charge transport materials: a SCAPS-1D study. *Multiscale and Multidisciplinary Modeling, Experiments and Design*, *8*(1), p.114.

[11] Yang, W.F., Igbari, F., Lou, Y.H., Wang, Z.K. and Liao, L.S., 2020. Tin halide perovskites: progress and challenges. *Advanced Energy Materials*, *10*(13), p.1902584.

[12] Slavney, A.H., Hu, T., Lindenberg, A.M. and Karunadasa, H.I., 2016. A bismuth-halide double perovskite with long carrier recombination lifetime for photovoltaic applications. *Journal of the American chemical society*, *138*(7), pp.2138-2141.

[13] Danladi, E., Oguzie, E.E. and Ezema, F.I., 2025. Challenges and outlooks on stability of inverted perovskite solar cells: a review insight. *Multiscale and Multidisciplinary Modeling, Experiments and Design*, *8*(1), p.119.

[14] Yang, J., Bao, C., Ning, W., Wu, B., Ji, F., Yan, Z., Tao, Y., Liu, J.M., Sum, T.C., Bai, S. and Wang, J., 2019. Stable, high-sensitivity and fast-response photodetectors based on lead-free Cs2AgBiBr6 double perovskite films. *Advanced Optical Materials*, *7*(13), p.1801732.

[15] Yin, L., Wu, H., Pan, W., Yang, B., Li, P., Luo, J., Niu, G. and Tang, J., 2019. Controlled cooling for synthesis of Cs2AgBiBr6 single crystals and its application for X-ray detection. *Advanced Optical Materials*, *7*(19), p.1900491.

[16] Lin, D., Zhan, Z., Huang, X., Liu, P. and Xie, W., 2022. Advances in components engineering in vapor deposited perovskite thin film for photovoltaic application. *Materials Today Advances*, *16*, p.100277.

[17] Shadabroo, M.S., Abdizadeh, H. and Golobostanfard, M.R., 2021. Dimethyl sulfoxide vapor-assisted Cs2AgBiBr6 homogenous film deposition for solar cell application. *ACS Applied Energy Materials*, *4*(7), pp.6797-6805.

[18] Yang, B., Chen, J., Yang, S., Hong, F., Sun, L., Han, P., Pullerits, T., Deng, W. and Han, K., 2018. Lead-Free Silver-Bismuth Halide Double Perovskite Nanocrystals. *Angewandte Chemie,* 57(19), pp. 5359-5363.

[19] Ullah, A., Shafiq, M., Abualnaja, K.M. and Fawy, K.F., 2025. The improvement in double perovskite solar cells Cs2AgBiBr6 by the praseodymium doping and surface passivation of polythiophene. *Chemical Engineering Science*, p.122384.

[20] Umer, S., Khan, M.I., Ullah, A., Asad, M., Kebaili, I., Mnif, W., Algarni, Z. and Saleem, M.I., 2024. Improving $Cs_2AgBiBr_6$ double perovskite solar cells through graphdiyne doping: A Stride towards enhanced performance. *Optical Materials,* 156, p. 115896.

[21] Danladi, E., Oguzie, E.E. and Ezema, F.I., 2025. Highly efficient 25.562% $Cs_2AgBiBr_6$ double perovskite solar cell with copper barium tin sulfide and ZnO as charge transport channels: an intuition from a theoretical study using SCAPS-1D. *Journal of Photonics for Energy*, *15*(2), pp.024501-024501.

[22] Khan, M.I., Farhat, L.B., Elhouichet, H. and Patil, R.P., 2025. Enhancing efficiency of $Cs_2AgBiBr_6$ double perovskite solar cells through bandgap reduction by molybdenum doping. *Journal of the Korean Ceramic Society*, *62*(2), pp.359-369.

[23] Lei, H., Hardy, D. and Gao, F., 2021. Lead-free double perovskite $Cs_2AgBiBr_6$: fundamentals, applications, and perspectives. *Advanced Functional Materials*, *31*(49), p.2105898.

[24] Yang, X., Chen, Y., Liu, P., Xiang, H., Wang, W., Ran, R., Zhou, W. and Shao, Z., 2020. Multifunctional Dye Interlayers: Simultaneous Power Conversion Efficiency and Stability Enhancement of $Cs_2AgBiBr_6$ Lead-Free Inorganic Perovskite Solar Cell through Adopting a Multifunctional Dye Interlayer. *Advanced Functional Materials*, *30*(23), p. 2001557.

[25] Zhao, X.G., Yang, D., Ren, J.C., Sun, Y., Xiao, Z. and Zhang, L., 2018. Rational design of halide double perovskites for optoelectronic applications. *Joule*, *2*(9), pp.1662-1673.

[26] Zhang, Z., Sun, Q., Lu, Y., Lu, F., Mu, X., Wei, S.H. and Sui, M., 2022. Hydrogenated $Cs_2AgBiBr_6$ for significantly improved efficiency of lead-free inorganic double perovskite solar cell. *Nature communications*, *13*(1), p.3397.

[27] Usman, A. and Bovornratanaraks, T., 2024. An extensive study of the impact of graphene passivation on HTLs (PTAA and NiO) in $MAPBI_3$ and $Cs_3Bi_2I_9$-based inverted perovskite solar cells for thermal stability in SCAPS 1D framework. *Solar Energy*, *284*, p.113043.

[28] Nikfar, N. and Memarian, N., 2022. Theoretical study on the effect of electron transport layer parameters on the functionality of double-cation perovskite solar cells. *Optik*, *258*, p.168932.

[29] Minbashi, M., Omrani, M.K., Memarian, N. and Kim, D.H., 2017. Comparison of theoretical and experimental results for band-gap-graded CZTSSe solar cell. *Current Applied Physics*, *17*(10), pp.1238-1243.

[30] Omrani, M.K., Minbashi, M., Memarian, N. and Kim, D.H., 2018. Improve the performance of CZTSSe solar cells by applying a SnS BSF layer. *Solid-state electronics*, *141*, pp.50-57.

[31] Minbashi, M., Ghobadi, A., Ehsani, M.H., Dizaji, H.R. and Memarian, N., 2018. Simulation of high efficiency SnS-based solar cells with SCAPS. *solar energy*, *176*, pp.520-525.

[32] Danladi, E., Gyuk, P.M., Tasie, N.N., Egbugha, A.C., Behera, D., Hossain, I., Bagudo, I.M., Madugu, M.L. and Ikyumbur, J.T., 2023. Impact of hole transport material on perovskite solar cells with different metal electrode: a SCAPS-1D simulation insight. *Heliyon*, *9*(6).

[33] Tariq, M.U.N., Masud, M.I., Al Dmour, H., Ghulman, H.A., Kashif, M., Malik, M. and Nahas, M., 2025. Optimization of high-efficiency solid-state dye sensitized solar cells (ssDSSCs) based on N719 dye via electron transport layer engineering using SCAPS-1D. *Results in Engineering*, p.106465.

[34] Danladi, E., Kashif, M., Daniel, T.O., Achem, C.U. and Gyan, M., 2022. 7.379% Power conversion efficiency of a numerically simulated solid-state dye-sensitized solar cell with copper (I) thiocyanate as a hole conductor. *East European Journal of Physics*, (3), pp.19-31.

[35] Danladi, E., Egbugha, A.C., Obasi, R.C., Tasie, N.N., Achem, C.U., Haruna, I.S. and Ezeh, L.O., 2023. Defect and doping concentration study with series and shunt resistance influence on graphene modified perovskite solar cell: a numerical investigation in SCAPS-1D framework. *Journal of the Indian Chemical Society*, *100*(5), p.101001.

[36] Hossain, M.K., Datta, A.K., Alsalman, O., Uddin, M.S., Toki, G.F., Darwish, M.A., Mohammad, M.R., Dwivedi, D.K., Haldhar, R. and Trukhanov, S.V., 2024. An extensive study on charge transport layers to design and optimization of high-efficiency lead-free Cs2PtI6-based double-perovskite solar cells: a numerical simulation approach. *Results in Physics*, *61*, p.107751.

[37] Lee, Y.M., Maeng, I., Park, J., Song, M., Yun, J.H., Jung, M.C. and Nakamura, M., 2018. Comprehensive understanding and controlling the defect structures: An effective approach for organic-inorganic hybrid perovskite-based solar-cell application. *Frontiers in Energy Research*, *6*, p.128.

[38] Noel, N.K., Stranks, S.D., Abate, A., Wehrenfennig, C., Guarnera, S., Haghighirad, A.A., Sadhanala, A., Eperon, G.E., Pathak, S.K., Johnston, M.B. and Petrozza, A., 2014. Lead-free organic–inorganic tin halide perovskites for photovoltaic applications. *Energy & Environmental Science*, *7*(9), pp.3061-3068.

[39] Hao, F., Stoumpos, C.C., Guo, P., Zhou, N., Marks, T.J., Chang, R.P. and Kanatzidis, M.G., 2015. Solvent-mediated crystallization of CH3NH3SnI3 films for heterojunction depleted perovskite solar cells. *Journal of the American Chemical Society*, *137*(35), pp.11445-11452.

[40] Xing, G., Mathews, N., Sun, S., Lim, S.S., Lam, Y.M., Grätzel, M., Mhaisalkar, S. and Sum, T.C., 2013. Long-range balanced electron-and hole-transport lengths in organic-inorganic CH3NH3PbI3. *Science*, *342*(6156), pp.344-347.

[41] Li, G., Zou, X., Cheng, J., Yu, X., Zhou, Z., Wang, J., Liu, B. and Chen, D., 2021. Simulation of carriers spatial distribution and transportation in co-mixing composition perovskite for solar cell. *Materials Research Express*, *8*(3), p.035006.

[42] Dipta, S.S., Uddin, A. and Conibeer, G., 2022. Enhanced light management and optimization of perovskite solar cells incorporating wavelength dependent reflectance modeling. *Heliyon*, *8*(11), p. e11380.

[43] Lazemi, M., Asgharizadeh, S. and Bellucci, S., 2018. A computational approach to interface engineering of lead-free CH 3 NH 3 SnI 3 highly-efficient perovskite solar cells. *Physical Chemistry Chemical Physics*, *20*(40), pp.25683-25692.

[44] Patel, P.K., 2021. Device simulation of highly efficient eco-friendly CH3NH3SnI3 perovskite solar cell. *Scientific reports*, *11*(1), p.3082.

[45] Son, D.Y., Im, J.H., Kim, H.S. and Park, N.G., 2014. 11% efficient perovskite solar cell based on ZnO nanorods: an effective charge collection system. *The Journal of Physical Chemistry C*, *118*(30), pp.16567-16573.

[46] Mamta, Kumari, R., Kumar, R., Maurya, K.K. and Singh, V.N., 2023. Ideal HTLs may open the door for further development of Sb2Se3 solar cells—a numerical approach. *Sustainability*, *15*(13), p.10465.

[47] Mortadi, A., Nasrellah, H., Monkade, M. and El Moznine, R., 2024. Investigation of bandgap grading on performances of perovskite solar cell using SCAPS-1D and impedance spectroscopy. *Solar Energy Advances*, *4*, p.100056.

[48] Sumona, F.B., Kashif, M., Danladi, E., Tighezza, A.M., Al-Mahmud, N., Toki, G.F., Pandey, R. and Hossain, M.K., 2023. Optimization of perovskite-KSnI3 solar cell by using different hole and electron transport layers: a numerical SCAPS-1D simulation. *Energy & Fuels*, *37*(23), pp.19207-19219.

[49] Kumar, M., Kumar, A., Raj, A., Kr. Singh, P. and Anshul, A., 2023, February. Effect of Band-Gap Tuning and Series Resistance on PCE of Optimized MAPbI3-Based PSC by SCAPS-1D Simulation. In *Macromolecular Symposia* (Vol. 407, No. 1, p. 2100464).

[50] Pang, B., Cui, W., Li, Y., Feng, J., Dong, H., Yu, L. and Dong, L., 2025. Lithium and sodium ion Co-doping: A promising strategy for enhancing the performance of Cs2AgBiBr6 perovskite solar cells. *Journal of Alloys and Compounds*, *1010*, p.177394.

[51] Srivastava, A., Kasliwal, M. and Shirage, P.M., 2025. From HTL to HTL-free: Experimental and numerically modelled performance dynamics of Cs2AgBiBr6 double perovskite solar cells. *Solar Energy*, *298*, p.113733.

[52] Yang, W., Li, W., Liu, Q. and Jin, Y., 2025. Design and simulation of gradient-structured Cs2AgBiBr6 carbon-based double perovskite solar cell for boosting photovoltaic performance. *Solar Energy*, *290*, p.113347.

[53] Mohandes, A., Moradi, M. and Nadgaran, H., 2021. Numerical simulation of inorganic $Cs_2AgBiBr_6$ as a lead-free perovskite using device simulation SCAPS-1D. *Optical and Quantum Electronics*, *53*(6), p.319.

[54] Alanazi, T.I., 2023. Design and device numerical analysis of lead-free Cs2AgBiBr6 double perovskite solar cell. *Crystals*, *13*(2), p.267.

[55] Chabri, I., Benhouria, Y., Oubelkacem, A., Kaiba, A., Essaoudi, I. and Ainane, A., 2023. Cs2AgBiBr6-based perovskite solar cell: A novel combination of ITO/CdS/Cs2AgBiBr6/CuAlO2/Pt, with inorganic charge transport layers. *Optik*, *274*, p.170560.

[56] Ukorah, I.N., Owolabi, A.J., Ali, H., Onimisi, M.Y., Tafida, R.A., Olalekan, A.J., Gambo, H.M., Usman, S.L., Christiana, A.O., Ukwenya, J.M. and Akinade, B.J., 2024. Investigating the Performance of TIN-Based Perovskite Solar Cell with Zinc Selenide as an ETM and Graphene as an HTM Using SCAPS-1D. *Progress in Physics of Applied Materials*, *4*(2), pp.171-181.